RAA 2018 Vol. **18** No. **7**, 82(12pp) doi: 10.1088/1674–4527/18/7/82

http://www.raa-journal.org *http://iopscience.iop.org/raa*

***R**esearch in*
***A**stronomy and*
***A**strophysics*

The optical/UV excess of X-ray-dim isolated neutron star II. Nonuniformity of plasma on a strangeon star surface

Wei-Yang Wang[1,2,3], Yi Feng[2,4,5], Xiao-Yu Lai[6], Yun-Yang Li[3], Ji-Guang Lu[4,7], Xuelei Chen[1,2,8] and Ren-Xin Xu[3,9]

[1] Key Laboratory of Computational Astrophysics, National Astronomical Observatories, Chinese Academy of Sciences, Beijing 100101, China; *wywang@bao.ac.cn*
[2] School of Astronomy and Space Sciences, University of Chinese Academy of Sciences, Beijing 100049, China
[3] School of Physics and State Key Laboratory of Nuclear Physics and Technology, Peking University, Beijing 100871, China
[4] National Astronomical Observatories, Chinese Academy of Sciences, Beijing 100101, China
[5] CAS Key Laboratory of FAST, National Astronomical Observatories, Chinese Academy of Sciences, Beijing 100101, China
[6] Hubei University of Education, Wuhan 430205, China
[7] Key Laboratory of Radio Astronomy, Chinese Academy of Sciences, Beijing 100101, China
[8] Center for High Energy Physics, Peking University, Beijing 100871, China
[9] Kavli Institute for Astronomy and Astrophysics, Peking University, Beijing 100871, China

Received 2017 November 17; accepted 2018 March 30

Abstract Several X-ray-dim isolated neutron stars (XDINSs), also known as the Magnificent Seven, exhibit a Planck-like soft X-ray spectrum. In the optical/ultraviolet (UV) band, there is an excess of radiation compared to an extrapolation from the X-ray spectrum. However, the majority exhibits "spectral deviations": the fact that there is more flux at longer wavelengths makes spectra deviate from the Rayleigh-Jeans law. A model of bremsstrahlung emission from a nonuniform plasma atmosphere is proposed in the regime of a strangeon star to explain the optical/UV excess and its spectral deviation as well as X-ray pulsation. The atmosphere is on the surface of strangeon matter, which has negligible emission, and is formed by the accretion of ISM-fed debris disk matter moving along the magnetic field lines to near the polar caps. These particles may spread out of the polar regions which makes the atmosphere non-uniform. The modeled electron temperatures are $\sim 100-200\,\mathrm{eV}$ with radiation radii $R_{\rm opt}^{\infty}\sim 5-14\,\mathrm{km}$. The spectra of five sources (RX J0720.4–3125, RX J0806.4–4123, RX J1308.6+2127, RX J1605.3+3249, RX J1856.5–3754) from optical/UV to X-ray bands can be fitted well by the radiative model, and exhibit Gaussian absorption lines at $\sim 100-500\,\mathrm{eV}$ as would be expected. Furthermore, the surroundings (i.e., fallback disks or dusty belts) of XDINSs could be tested by future infrared/submillimeter observations.

Key words: X-rays: stars — stars: neutron — stars: individual

1 INTRODUCTION

The Magnificent Seven (hereafter referred to as Seven) refers to seven X-ray-dim isolated neutron stars (XDINSs) with thermal radiation in the form of soft X-rays, which offer an unprecedented opportunity to unveil their surface temperature and magnetic field as well as the state of dense matter at supra nuclear densities (Turolla 2009). They are located in the upper right corner of the $P-\dot{P}$ diagram together with a few high-B pul-

sars and magnetars, indicating that they may have strong magnetic fields (Mori & Ruderman 2003; Tong 2016). These objects, including RX J1856.5–3754 (J1856 hereafter), are characterized by Planck-like spectra (with no power law component) in the X-ray band with a relatively steady flux over long timescales (Burwitz et al. 2001; Ho et al. 2007; van Kerkwijk & Kaplan 2007; Kaplan & van Kerkwijk 2009). Compared with the extrapolated blackbody X-ray spectrum, an XDINS exhibits excess in optical/ultraviolet (UV) flux, by a factor of $\sim 5-50$ (Kaplan et al. 2011). However, it is *not an alleged* observation that the optical flux appears to deviate from a Rayleigh-Jeans (R-J) distribution. The spectrum can be described as power law emission ($F_\nu \propto \nu^\beta$). Compared to an R-J spectrum with $\beta = 2$, the spectra for XDINS are flatter (Kaplan et al. 2011), with the only exception being RX J0420.0–5022. Also noteworthy is the fact that the spectral deviations of most XDINSs are greater than the photoelectric absorptions by neutral hydrogen as modeled from X-ray spectra. Certainly, more powerful observations would verify if these deviations are real, but here we focus on understanding the flat spectrum.

To explain the optical excess, in the regime of a conventional neutron star (NS), authors propose two representative models.

(1) Trümper et al. (2004) and Turolla et al. (2004) adopted a model of a "bare" (i.e., no gaseous atmosphere sits on the top of the crust) NS, the spectrum of which can be described as a two-component blackbody. In the case of J1856 (at a distance $d \sim 120\,\mathrm{pc}$ from us), for example, the temperature of the hot spot is $kT_{\rm X}^{\infty} \sim 63.5\,\mathrm{eV}$ with radiation radius $R_{\rm X}^{\infty} \sim 4.4\,(d/120\,\mathrm{pc})\,\mathrm{km}$, while the cold part has $kT_{\rm opt} < 33\,\mathrm{eV}$ and $R_{\rm opt}^{\infty} > 17\,(d/120\,\mathrm{pc})\,\mathrm{km}$ (Burwitz et al. 2003; Trümper et al. 2004).

They are fine tuning the geometry in order to explain the small X-ray pulsed fraction (PF) observed, PF $< 1.3\%$. Recently, the gravitational wave observation of GW170817 provided valuable constraints on tidal deformability, $\Lambda(1.4\,M_\odot) < 10^3$ (Abbott et al. 2017). According to this result, Annala et al. (2017) concluded that the maximal radius is $\sim 14\,\mathrm{km}$ if the speed of sound for the NS is smaller than $c/\sqrt{3}$, with c being the speed of light. Therefore, an NS with large radius ($> 17\,\mathrm{km}$) is not acceptable.

(2) Ho et al. (2007) proposed a model with a thin, magnetic, partially ionized hydrogen atmosphere on top of a condensed iron surface to fit the spectrum of J1856. However, a condensed surface at the bottom of the atmosphere brings more low-energy photons so that it has to introduce a large value of hydrogen absorption that would consequently present a strong photoelectric absorption which deviates from the R-J spectrum of J1856 at optical bands. Additionally, both of these two NS models face a common problem that the cohesive energy for iron atoms and molecular chains in strong magnetic fields is quite uncertain since this small number is the difference between two large numbers (Mueller 1984).

However, the inner structure of the pulsar remains unclear, which depends on the challenging problem of fundamental strong interaction at low energy scale. There are thus many speculations, among which a strangeon star model is proposed to understand the differing manifestations of compact objects (Lai & Xu 2017). A bremsstrahlung radiative model of a strangeon star atmosphere was proposed to explain the optical/UV excess (Wang et al. 2017). The atmosphere is modeled with two temperature components (Xu 2014), formed and maintained by accretion, and can be simply considered as the upper layer of a normal NS. The radiation is optically thick at optical bands but optically thin at X-ray bands. Thus, the observed spectra of the Seven can be fitted well by the radiative model, from optical to X-ray bands, except for spectral deviations from the R-J regime at optical/UV bands.

In this paper, we propose that the spectral deviations come from non-uniformities in the atmosphere, which is on top of an emission-negligible strangeon star surface. The fallback disk matter that is accreted moves along the magnetic field lines to near the polar caps, and some part may diffuse to other regions, generating a nonuniform distribution in the atmosphere. Thus, the spectrum may deviate from R-J radiation at optical bands because the bremsstrahlung emissivity is particle distribution-dependent (as demonstrated in Fig. 2).

In Section 2.1, we assert that the strangeon matter could have negligible emission. In Section 2.2, we propose a toy model to describe the non-uniformity of the atmosphere and show that this distribution could make the spectrum deviate from the R-J regime. In Section 3, we present the fitting details and results for the X-ray data (Sect. 3.1) and optical data (Sect. 3.2). Finally, we discuss various issues related to this model in Section 4, and make a brief summary in Section 5.

2 RADIATION FROM A STRANGEON STAR

2.1 The Strangeon Star Surface

The radiation from strangeon matter is totally neglected in the calculation as follows, and this could be valid because of the high plasma frequency, $\omega_{\rm p}$. The plasma frequency of a degenerate charged Fermion gas is $\omega_{\rm p} \propto n^{1/3}$, with n the number density (Usov 2001). For strangeon matter with baryon density, $n_{\rm b}$, to be a few times the nuclear density, the electron number density $n_{\rm e} = (10^{-5} \sim 10^{-6})n_{\rm b}$, with baryon number density $n_{\rm b} = (1.5 - 2.0)n_{\rm nuc}$, where $n_{\rm nuc}$ is the normal nuclear matter density (Alcock et al. 1986), then the frequency $\omega_{\rm p} \sim 100\,{\rm keV}$ must be so high that the optical as well as soft X-ray emissivity is negligible. Therefore, the strangeon star's atmosphere could be similar to the upper layer of a normal NS, but differences do exist (Fig. 1). The emission-negligible surface does not radiate a lot of high energy photons, which coincides with the fact that the high energy tail in the X-ray spectrum of XDINSs is absent (e.g., van Kerkwijk et al. 2007).

However, the strangeon matter surface exhibits an extremely high reflectance that can be regarded as total reflection. The reflected component by the strangeon matter surface should certainly be included in the total emission. Then, the observed flux is multiplied by a factor of $[1 + \exp(-\tau_\infty)]$, where the factor $\exp(-\tau_\infty)$ results from the reflection (see Appendix) and is illustrated in Figure 1. The reflection effect intensifies X-ray emissions but can be ignored in optical bands.

2.2 The Nonuniform Plasma Atmosphere: A Toy Model

A nonuniform plasma atmosphere could produce a bremsstrahlung radiation spectrum that deviates from the R-J law at low energy (optical/UV) bands, because the optical depth of the radiation is energy-dependent (Wang et al. 2017). The total flux is the sum of radiation from local regions (see Eq. (A.3) in the Appendix). In these cases, a nonuniform atmosphere may enable the spectral index to depart from an R-J spectrum. A sample of spectra differing from a nonuniform atmosphere is shown in Figure 2. It is worth noting that the radiation in high energy is mainly from the polar caps. Therefore, the data from both high energy and low energy can be fitted separately (see Sect. 3). Actually, the observed flux is the time-averaged radiation from a rotating NS and the detailed calculations are shown in the Appendix.

Note that the temperature gradient could not be the reason for the deviation because of the high thermal conductivity of the star's surface, unless there is an extremely strong magnetic field ($\sim 10^{15}$ G, e.g., Pons et al. 2009). Thus, we regard non-uniformity in the number density as the main reason for the fact that the spectral index deviates. However, a Goldreich-Julian-like distribution (Goldreich & Julian 1969) in a dipolar magnetic field cannot explain such anomalous behavior because the regions that have low density radiative matters are very small. There are some possible reasons for the non-Goldreich-Julian-like distribution: (i) some atmospheric matter gyrates around the magnetic lines and diffuses to other regions; (ii) there are some multipolar magnetic fields that support particles moving into high latitude regions from polar caps.

As we have discussed in Section 2.1, the atmospheric matter is accreted by gravity and moves along the magnetic field lines to near the polar caps. However, there may be some multipolar magnetic fields that help small parts of the accreted matters spread out near polar caps and exhibit a nonuniform particle distribution. Here, based on the above analysis, it is assumed that the atmosphere: i) is approximately uniform at the polar caps; ii) can be described by a power-law-like distribution at high latitudes; iii) deceases rapidly at the edges of the polar caps. To simply account for the complicated atmospheric distribution in the magnetosphere, we propose a toy model to describe the nonuniformity. An assumed distribution with number density can be constructed,

$$\begin{aligned} n_{\rm e} &= n_{\rm i} = n_{\rm i0}(\theta)\exp\left(\frac{-m_{\rm i}gz}{kT_{\rm i}}\right) \\ &= n_0\frac{\exp\left(-\frac{m_{\rm i}gz}{kT_{\rm i}}\right)}{1+\xi\cdot\theta^\gamma}, \end{aligned} \tag{1}$$

where z measures the height above the star's surface, n_0 is the number density of ions on the star's surface at $\theta = 0$, $m_{\rm i}$ is the mass of an ion (mainly proton), $T_{\rm i}$ is the temperature of ions, g is the gravitational acceleration above the surface of a strangeon star, and ξ as well as γ are two constants to describe the nonuniformity, respectively. The combination term $\xi \cdot \theta^\gamma$ describes the behavior near the polar cap. In this case, the plasma atmosphere would be approximately uniform if all the matter accreted by the interstellar medium (ISM)-fed debris disk could diffuse from the polar caps to other parts of the stellar surface (i.e., $\xi = 0$, where an R-J spectrum is shown at optical

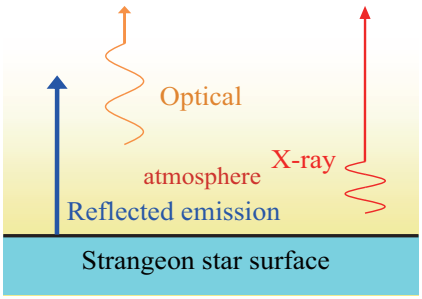

Fig. 1 A schematic diagram of the observed radiation from the atmosphere which is on top of a strangeon star. The total observed radiation consists of emission from the atmosphere and the reflected component from the surface where emission is negligible. The radiation is optically thin at X-ray bands so that photons can be emitted from a much deeper location but it is optically thick for long wavelength photons.

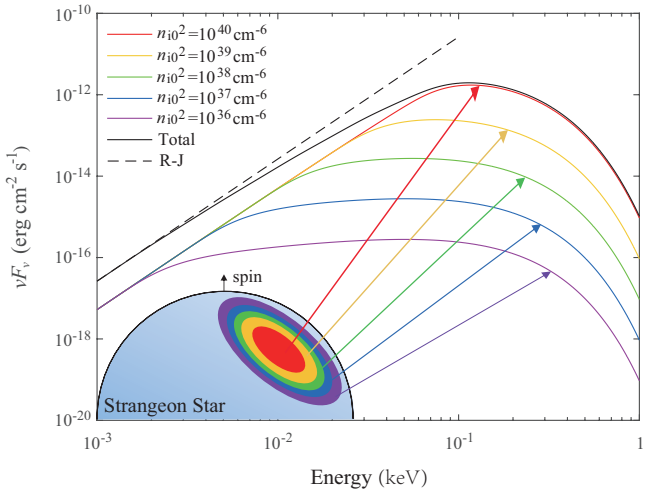

Fig. 2 The observed spectrum of a rotating NS with a nonuniform atmosphere. The total radiation consists of five components with the same radiative areas but different number densities: $n_{i0}^2 = 10^{40}\ \mathrm{cm}^{-6}$ (*red solid line*), $n_{i0}^2 = 10^{39}\ \mathrm{cm}^{-6}$ (*yellow solid line*), $n_{i0}^2 = 10^{38}\ \mathrm{cm}^{-6}$ (*green solid line*), $n_{i0}^2 = 10^{37}\ \mathrm{cm}^{-6}$ (*blue solid line*) and $n_{i0}^2 = 10^{36}\ \mathrm{cm}^{-6}$ (*purple solid line*), for given $T_\mathrm{e} = 0.1\,\mathrm{keV}$, $T_\mathrm{i} = 0.1\,\mathrm{MeV}$ and $(R_\mathrm{opt}^\infty/d)^2 = (10\,\mathrm{km}/0.25\,\mathrm{kpc})^2$. The total radiation (*black solid line*) of these five components exhibits deviation compared with an R-J spectrum (*dashed line*).

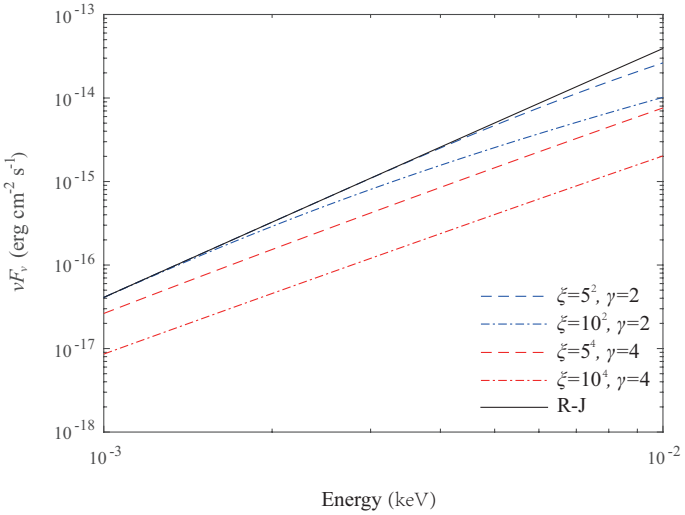

Fig. 3 Comparison of photo indexes for the spectrum with $\xi = 5$, including $\gamma = 2$ (*blue dashed line*) and $\gamma = 4$ (*red dashed line*), and the corresponding case $\xi = 10$ with $\gamma = 2$ (*blue dash-dotted line*) and $\gamma = 4$ (*red dash-dotted line*). The *solid line* is an R-J spectrum from a uniform atmosphere.

bands). In order to show the impacts of ξ and γ on the spectral index, we calculate the observed time-averaged spectrum with $kT_{\rm e} = 0.1\,{\rm keV}$, $n_0^2 kT_{\rm i} = 10^{42}\,{\rm keV\,cm^{-6}}$, $(R_{\rm opt}^{\infty}/d)^2 = (10\,{\rm km}/0.25\,{\rm kpc})^2$, $\zeta = 0$ and $\alpha = 0$ (for definitions of ζ and α, see the Appendix). A comparison of deviations with different ξ and γ is shown in Figure 3.

3 DATA REDUCTION AND FITTING

3.1 X-ray Data

The details of X-ray data reduction from *XMM-Newton* for the Seven can be found in Wang et al. (2017). Spectral analysis for the XDINS is performed with XSPEC 12.9 (Arnaud 1996), by selecting photon energies in the range of 0.1–1.0 keV. To exclude some degeneracies, two angles, ζ and α, are treated as zero because the spectra will not be felt in the range $\zeta < 30^{\rm o}$ and $\alpha < 15^{\rm o}$. In addition, there is little decrease in flux with ζ and α increasing while the spectral index does not increase.

The optical and X-ray data can be fitted separately because the emission is optically thin at high-energy bands but optically thick at optical bands. We first fit X-ray data with the uniform atmosphere model accounting for polar caps mainly emitting high energy photons. The results of spectral fitting by the uniform model with Gaussian absorption are presented in Wang et al. (2017). Therefore, we fix $N_{\rm H}$, $T_{\rm e}$ and $E_{\rm Line}$ as the modeled uniform atmosphere while setting y/R (where $y = n_{\rm i0}^2 kT_{\rm i}$, R is assumed to be $R_{\rm opt}^{\infty}$) and width σ as free parameters. Then we treat all these fixed parameters as free, and extract the best-fit $N_{\rm H}$ to fix photoelectric absorption.

3.2 Optical Data

Optical counterparts for each XDINS have been searched in deep optical observations by the *Hubble Space Telescope* (*HST*), and detailed photometry measurements and data errors are presented in Kaplan et al. (2011). Each photometry spectrum of XDINS can be fitted by a power law and fixed by a function of extinction in which the value is determined by the column density of hydrogen $N_{\rm H}$ from fitting X-ray spectral data (details on XSPEC photoelectric absorption are provided in Morrison & McCammon 1983).

To describe photoelectric absorption when the light is transmitted through an extinction layer, the atmospheric extinction, expressed in magnitude A_λ, is defined (see, Cardelli & Ackerman 1983, eq. (3)), and optical extinction A_V depends on $N_{\rm H}$ which is given by X-ray spectral fitting: $A_V = N_{\rm H}/1.79 \times 10^{21}\,{\rm cm^{-2}}$ (Predehl & Schmitt 1995). In general, the extinction value A_λ/A_V depends on wavelength and the value of the overall extinction A_V. However, A_λ/A_V can be considered as wavelength-dependent since the changes are less than 1% in A_λ/A_V for the range $N_{\rm H} = (1-4) \times 10^{20}\,{\rm cm^{-2}}$ (Kaplan et al. 2011). The absorbed flux can be described as

$$F_\nu = F_{\nu 0} \cdot 10^{-2.23 \frac{A_\lambda}{A_V} \cdot \frac{N_{\rm H}}{10^{22}\,{\rm cm^{-2}}}},$$

where $F_{\nu 0}$ is the unabsorbed flux. van Kerkwijk & Kulkarni (2001a) present approximate wavelength-dependent values of A_λ/A_V for an unabsorbed 10^6 K($\sim$ 100 eV) blackbody.

Then, with fixed photoelectric absorption, the optical data are fitted by nonuniform radiative models. In this process, the optical data are fitted by the absorbed nonuniform radiative model with free $R_{\rm opt}^{\infty}$ as well as fixed ξ and γ. Some optical properties are listed in Table 1.

Table 1 Summary of Photometry and Some Parameters Describing XDINSs

Source	Optical (mag)	β	PF (%)
J0420	$B = 26.6$	2.20 ± 0.22	13
J0720	$B = 26.6$	1.43 ± 0.12	8–15
J0806	$B > 24$	1.63 ± 0.20	6
J1308	$m_{\rm 50ccd} = 28.6$	1.62 ± 0.14	18
J1605	$B = 27.2$	1.23 ± 0.07	–
J1856	$B = 25.2$	1.93 ± 0.08	< 1.3
J2143	$B > 26$	0.53 ± 0.08	4

Notes: The optical data quoted from Kaplan et al. (2011) for each XDINS can be fitted by a power law ($F_\nu \propto \nu^\beta$, where β is the photo index). The optical stellar magnitude and PF shown in this table are quoted from Haberl (2007).

We list the values of ξ and γ that are at $\geq 1\sigma$ confidence and the modeled $R_{\rm opt}^{\infty}$ in Table 2. With these parameters, the radiative spectra and spectral data of J0720, J0806, J1308, J1605 and J1856 are reproduced and plotted in Figure 4. The X-ray data are also fitted by the blackbody model, but only J1856 shows a better fit ($\chi^2 = 1.11$) than the bremsstrahlung emission.

Therefore, the spectra of J1308 and J1856 can be fitted well by R-J-like emissions which are photoelectrically absorbed without nonuniformity. For J1605, X-ray data fitting with a uniform radiative model presents a large value of $N_{\rm H} \sim 3 \times 10^{20}\,{\rm cm^{-2}}$. In this case, the absorbed nonuniform emission can fit the deviating spectrum well. However, the nonuniform radiation predicts that $N_{\rm H}$ would be smaller than $\sim 1.5 \times 10^{20}\,{\rm cm^{-2}}$ because the nonuniformity of the atmosphere decreases

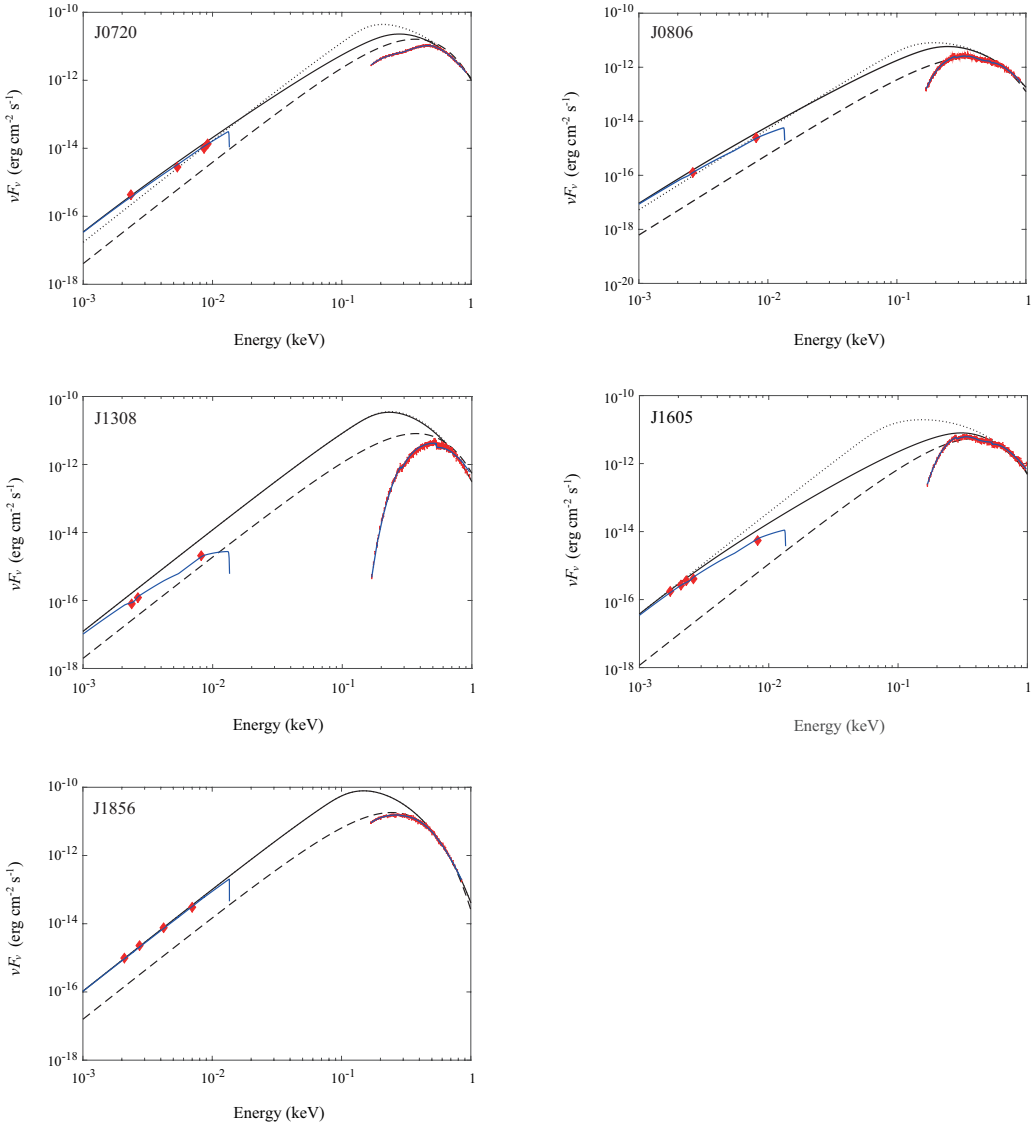

Fig. 4 The spectra of J0720 (*top left*), J0806 (*top right*), J1308 (*center left*), J1605 (*center right*) and J1856 (*bottom*) from optical to X-ray bands are shown in this figure. The absorbed best-fit nonuniform radiative model for each source is the *blue solid line*, while the unabsorbed nonuniform radiative model is the *black solid line*. To exhibit the optical/UV excesses, a pure blackbody (*black dashed line*) extrapolated from each X-ray spectrum is plotted. The archival X-ray data with their error bars from *XMM-Newton* (*red dots*) and optical data (*red diamonds*) from the *HST* are also plotted. By comparison, the uniform radiative model (*black dotted line*) is also plotted.

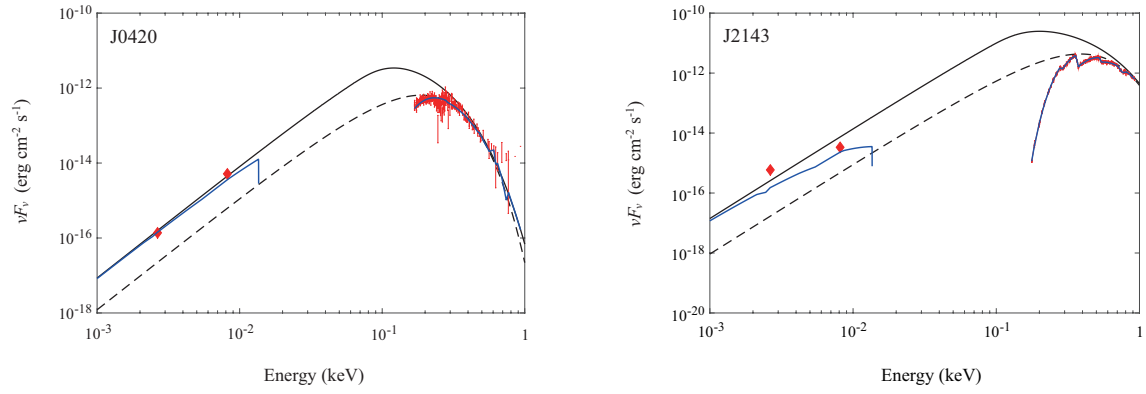

Fig. 5 Same as Fig. 4 but for J0420 (*left*) and J2143 (*right*). The uniform radiative model is the *black solid line*.

Table 2 The Parameters Obtained from X-ray Spectral Fitting

Source RX	$kT_{\rm e}$ (eV)	$R^{\infty}_{\rm opt}$ (km)	y ($\times10^{42}\,{\rm cm}^{-6}\,{\rm keV}$)	$E_{\rm line}$ (eV)	$N_{\rm H}$ ($\times10^{20}\,{\rm cm}^{-2}$)	d (pc)	ξ ($\times10^{2}$)	γ	χ^2/dof
(1)	(2)	(3)	(4)	(5)	(6)	(7)	(8)	(9)	(10)
J0420.0−5022	71.6 ± 2.5	9.3 ± 0.3	1.49 ± 0.25	250	1.60 ± 0.47	345	–	–	1.15/131
J0720.4−3125	179.0 ± 2.2	13.5 ± 0.1	37.3 ± 2.21	217.8 ± 20.3	1.02 ± 0.33	360	2.5	5	1.43/199
J0806.4−4123	165.8 ± 5.8	4.5 ± 0.2	5.00 ± 0.82	445.8 ± 4.3	3.26 ± 0.19	250	1.5	3	1.01/423
J1308.6+2127	131.4 ± 2.4	12.0 ± 0.2	10.46 ± 1.13	408.9 ± 3.4	8.77 ± 0.19	500	0	–	1.05/285
J1605.3+3249	181.1 ± 6.5	13.9 ± 0.5	1.12 ± 0.18	445.2 ± 4.7	3.28 ± 0.18	390	5.0	3	1.12/320
J1856.5−3754	96.2 ± 1.1	12.8 ± 0.1	2.11 ± 0.15	110.5 ± 56.9	0.68 ± 0.26	160	0	–	1.13/297
J2143.0+0654	158.0 ± 3.7	11.7 ± 0.2	10.37 ± 1.29	759.0 ± 11.1	8.36 ± 2.41	430	>1	>1	1.14/225

Notes: Columns (1)–(10) are source name (Source RX), temperature of electrons ($kT_{\rm e}$), radius of stars ($R^{\infty}_{\rm opt}$), parameter y, energy of Gaussian absorption lines, neutral hydrogen column density ($N_{\rm H}$), distance (d), ξ, γ and χ^2/degree of freedom respectively. Errors in the spectral model parameters are derived for a 90% confidence level. The distances are from Kaplan & van Kerkwijk (2009). The absorption line for J0420 is fixed. J2143 also shows an edge at $E_{\rm edge}=365.6\pm2.2\,{\rm eV}$ with $\tau=1.07\pm0.07$.

the emissions from polar caps in low-energy X-ray bands ($\sim0.1-0.4\,{\rm keV}$). This is the same as the case J0806 in that $N_{\rm H}$ is estimated to be $\sim\ 2.2\times10^{20}\,{\rm cm}^{-2}$, which is supposed to be smaller than the Galactic value of $2.7\times10^{20}\,{\rm cm}^{-2}$ obtained from Kalberla et al. (2005). However, J1308 shows a larger value of $N_{\rm H}$ that may indicate a long distance from us or a much denser interstellar surrounding. The observation of this source shows a high PF ($\sim18\%$, Kaplan & van Kerkwijk 2005) that leads to large fitting errors, and the gravitational redshift of this source is $\sim\ 0.16$ which demonstrates $(M/M_{\odot})/(R/1\,{\rm km})\sim0.87$, indicating a stiff equation of state for the NS (Potekhin et al. 2016).

The faintest X-ray source among the Seven, J0420, shows a steeper spectrum ($\beta=2.20\pm0.22$ which is greater than the case in the R-J regime) at optical/UV bands that is different from other XDINSs. This large photo index may result from the large value of PF (a factor of $\sim\ 13\%$) which is revealed by fitting a sine wave to the X-ray pulse profile (Haberl et al. 2004). The data and spectral fitting by the uniform atmosphere model of J0420 and J2143 are reproduced and plotted in Figure 5. In addition, J2143 shows a flatter optical spectrum ($\beta=0.53\pm0.08$). One possible reason for the flat spectrum is that a strong magnetic field ($\gtrsim10^{15}\,{\rm G}$, e.g., Pons et al. 2009) blocks atmospheric matter, making diffusion difficult. In this case, the temperature gradient should be considered (similar to a multi-color blackbody spectrum of a black hole accretion disk which presents a spectral index of ~0.33 at low energy bands), or there may be a high toroidal magnetic field that blocks transmission of heat (Geppert et al. 2006). Almost all of the accreted matter cannot spread out from the small polar regions which also leads to an extremely thin atmosphere. We use the uniform radiative model with an absorption edge and Gaussian absorption to fit the X-ray data of J2143. The best fitting result shows two absorptions, $E_{\rm edge}=365.6\pm2.2\,{\rm eV}$ with $\tau=1.07\pm0.07$, and $E_{\rm line}=759.0\pm11.1\,{\rm eV}$. These absorptions may predict a strong magnetic field.

Five spectra from the Seven can be fitted well by the radiative model, from optical/UV to X-ray bands, and exhibit absorption lines (discussions of these lines can be seen in Wang et al. 2017). In addition, we plot the absorbed bremsstrahlung and blackbody radiations to demonstrate the optical/UV excess of XDINS (see Fig. 4).

4 DISCUSSION

4.1 The Accretion and Evolution of XDINSs

XDINSs can accrete matter from fallback disks. The fallback disk may be fed by ISM-matter, which then becomes a so-called ISM-fed debris disk accretion (IFDA). In a generalized IFDA model, the NS accretes from a thin fallback disk in the early phase through the propeller mechanism and transforms to thick-disk accretion or spherical accretion in the late phase as the disk depletes and the ISM dominates the accretion. The radiation is supposed to come from accreted matter from the ISM-fed debris disk on the stellar surface instead of the disk. As a magnetic and accreting NS, the X-ray luminous accreted matter is a small fraction of incoming matter originating from the disk. Thus, the accretion rate at Alfvén radius $\dot{M}_{\rm A}$ should be larger than the X-ray luminous accretion rate $\dot{M}_{\rm X}\sim10^{10}-10^{11}\,{\rm g\,s}^{-1}$ by a factor of $10-100$ (Toropina et al. 2001). With a weak magnetic field of $10^8\,{\rm G}\lesssim B\lesssim10^{10}\,{\rm G}$, the Alfvén radius $R_{\rm A}=(\frac{R^6B^2}{\dot{M}_{\rm A}\sqrt{2GM}})^{2/7}\lesssim10^{10}\,{\rm cm}$ and the Bondi radius $R_{\rm B}\sim10^{12}\,{\rm cm}$ can be calculated (Wang et al.

2017). For such a slowly rotating NS, the light cylinder radius is calculated to be $R_{\rm LC} \sim 10^{10}$ cm. In case of $R_{\rm A} < R_{\rm LC} < R_{\rm B}$, the inflowing matter would be accreted along the magnetic field lines to near the polar caps and observed in simulations of disk accretion (Long et al. 2007; Romanova et al. 2018). The relationship of $\dot{M}_{\rm A} > \dot{M}_{\rm X} > \dot{M}_{\rm B}$ implies that the inflowing matter is sufficient to maintain the radiation. The disk mass can be estimated as

$$M_{\rm D} = \int_{R_{\rm A}}^{R_{\rm B}} 2\pi\Sigma r^2 dr \sim 10^{-10} M_\odot, \qquad (2)$$

where Σ is the standard disk density. The disk mass is much smaller than a typical initial mass of $0.1\,M_\odot$ which implies the disk has experienced long term depletion. In the late phase of the IFDA model, the X-ray luminous accretion rate is around the Bondi accretion rate of $\dot{M}_{\rm X} \simeq \dot{M}_{\rm A} \simeq \dot{M}_{\rm B} \simeq 10^8\,{\rm g\,s^{-1}}$. As a result, isolated NSs at the late phase of IFDA exhibit X-ray luminosities of $\sim 10^{29}\,{\rm erg\,s^{-1}}$ that are too faint to be detected unless they are at nearby distances. Detections of these NSs are expected from future high-resolution X-ray surveys and gravitational microlensing.

Considering gravitational capture at $R_{\rm A}$, the luminosity at $R_{\rm A}$ is $L_{\rm A} = (3/2)GM\dot{M}_{\rm A}/R_{\rm A} = 10^{27} - 10^{28}\,{\rm erg\,s^{-1}}$. The effective temperature $T_{\rm A} = [L_{\rm A}/(4\pi R_{\rm A}^2\sigma)]^{1/4} \sim 0.1$ eV, which is estimated by gravitational capture, is an upper limit. In this case, the contribution from the disk to optical/UV emission (as well as X-ray) can be ignored. Also, the X-ray absorption is supposed to be neglected because the density might be very low in the geometrically thick depleting disk.

When the magnetospheric radius $\sim R_{\rm A}$ is larger than the corotation radius $R_{\rm Co} = (GM/\Omega)^{1/3} \sim 10^8$ cm, the NS is in a so-called "propeller" stage (Davidson & Ostriker 1973; Illarionov & Sunyaev 1975). Thus, one can obtain the braking torque (Menou et al. 1999; Chatterjee et al. 2000)

$$N = 2\dot{M}_{\rm A} R_{\rm A}^2 \Omega_{\rm K}(R_{\rm A})\Big[1 - \frac{\Omega}{\Omega_{\rm K}(R_{\rm A})}\Big], \qquad (3)$$

where Ω is the angular frequency of the NS and $\Omega_{\rm K}(R_{\rm A}) = \sqrt{GM/R_{\rm A}^3}$ is the Keplerian angular frequency at $R_{\rm A}$. Therefore, the estimated spin-down rate of $\dot{P} \sim 10^{-14}\,{\rm s\,s^{-1}}$ is consistent with observation.

4.2 Nonuniformity of the Atmosphere

In Section 2.2, we propose that a nonuniform atmosphere would lead to spectral index deviation. Before that, we tried to use a distribution of a cos function (i.e., a Goldreich-Julian distribution) to fit the spectrum. The reason why a cos function failed is that the radius of the polar cap is very large so that there are too many higher energy photons. If the deviation originated from the temperature gradient (e.g., two components of a blackbody), there would be a lower temperature $T \lesssim 10^5$ K component that deviates from the calculation assuming low thermal conductivity on the star's surface. One possible reason is a high crustal toroidal magnetic field $B_{\rm tor} \sim 10^{15}$ G that blocks the heating transfer (Geppert et al. 2006). In terms of the nondeviating optical spectrum (i.e., R-J spectrum), the observed optical depth $\tau_\infty \gtrsim 1$ at $\sim 10\,{\rm eV}$ leads to the surface number density $n_{\rm i0}(\theta) \gtrsim 10^{17}\,{\rm cm^{-3}}$. In fact, falling atoms move along the magnetic field lines to near the polar caps, and collisions between ions and electrons may make them diffuse across the magnetic field lines. The atmosphere would be spherically symmetrical (i.e., uniform) if these charged particles could quickly spread around the whole surface.

In case the Seven rotate slowly, the diffusion of these charged atmospheric particles can be regarded as one-dimensional on the stellar surface. The timescale of the collision between an ion and an electron is

$$t_{\rm ie} = \frac{3(kT_{\rm e})^{1.5} m_{\rm e}^{0.5}}{4\sqrt{2\pi} e^4 n_{\rm e} \ln\bar{\Lambda}} \sim 10^7 \frac{1\,{\rm cm^{-3}}}{n_{\rm e}}\,{\rm s}, \qquad (4)$$

where $\ln\bar{\Lambda}$ is a factor of ~ 10 for the plasma atmosphere. Accounting for diffusion of the plasma, we have

$$-\nabla p - n_{\rm e} e \boldsymbol{u} \times \boldsymbol{B} - \frac{m_{\rm e} n_{\rm e} \boldsymbol{u}}{t_{\rm ie}} = m_{\rm e} n_{\rm e} \frac{d\boldsymbol{u}}{dt}, \qquad (5)$$

where p is pressure of the plasma, $\boldsymbol{u}$ is the velocity of electrons and $\boldsymbol{B}$ is the local magnetic field in a vertical direction. From Equation (5), the current density can be regarded as

$$\boldsymbol{J} = n_{\rm e}\boldsymbol{u} = -\frac{D}{R}\frac{\partial n_{\rm e}}{\partial\theta}\hat{\boldsymbol{\theta}}, \qquad (6)$$

where D is defined as the diffusion coefficient and $\hat{\theta}$ the local orthogonal unit vectors in the directions of increase.

Actually, the effect of ambipolar diffusion must be considered because the mass of ions is greater than that of electrons. For a two-temperature atmosphere when $B > 10^8$ G, the ambipolar diffusion coefficient

$$D_{\rm A} = \Big(1+\frac{T_{\rm i}}{T_{\rm e}}\Big)\frac{kT_{\rm e}t_{\rm ie}}{m_{\rm e}\Big(1+\omega_c^2 t_{\rm ie}^2\Big)} \sim 10^4 \frac{n_{\rm e}}{1\,{\rm cm^{-3}}}\Big(\frac{1\,{\rm G}}{B}\Big)^2, \qquad (7)$$

where ω_c is the Larmor frequency. Diffusion is blocked by a Lorentz force with a strong magnetic field near the polar cap. However, regarding this case as a dipole magnetic field, with an increase of θ, collision between ions and electrons may play a leading role in blocking the diffusion against the magnetic field. Certainly, there are still small parts that have non-strange accreted matter which could permeate into the interior of the star, i.e., penetrating the strangeness barrier. The penetration timescale of ions when there is a stable equilibrium between accretion and permeation for these falling ions is $\tau_{\rm p} \sim \Delta M/\dot{M}_{\rm X} \sim 0.1 - 10^5$ s (Wang et al. 2017). As the electrons diffuse across magnetic field lines, spreading over almost the entire stellar surface with a low penetration, a stable diffusion equation can be described as

$$\frac{\partial n_{\rm e}}{\partial t} = \frac{D_{\rm A}}{R^2}\frac{1}{\sin\theta}\frac{\partial}{\partial\theta}\Big(\sin\theta\frac{\partial n_{\rm e}}{\partial\theta}\Big) - \frac{n_{\rm e}}{\tau_{\rm p}}. \qquad (8)$$

The solution of $n_{\rm e}$ can be fitted well by a single power law distribution at high latitude regions. It is advisable that we use the toy model instead of a complete numerical solution of Equation (5). The nonuniform toy model may predict that multipole magnetic fields would be on the surface. Then, the accreted particles move along this magnetic field into high latitude regions from near the polar caps.

Here, a typical diffusion length of particles which can diffuse over the whole stellar surface would be

$$L = \sqrt{D_A \tau_{\rm p}} \gtrsim R\,. \qquad (9)$$

With a number density of $n_{\rm e} \sim 10^{22}\,{\rm cm}^{-3}$ and $R \sim 10$ km, one can infer that there is a weak magnetic field ($10^8\,{\rm G} \lesssim B \lesssim 10^{10}\,{\rm G}$) on the surface. In fact, XDINSs are radio quiet and show purely thermal X-ray emissions that suggest their magnetospheres may be not active. However, they are located in the upper right corner of the $P - \dot{P}$ diagram ($B \sim 10^{12} - 10^{14}\,{\rm G}$) and beyond the death line to be "active" NSs. The reason why the real magnetic field is smaller than the $P - \dot{P}$-inferred magnetic field is that the propeller torque of a fallback disk may modify the period derivative (Liu et al. 2014). Additionally, there may be some diffusions in the magnetosphere before matter accretes onto the stellar surface so that a weak magnetic field is estimated.

The X-ray optically thin atmosphere presents some faint absorption lines which may be derived from hydrocyclotron oscillation (Xu et al. 2012) in spectra. These absorption lines can be fitted well by single Gaussian absorptions with width $\sigma \sim 0.05$ keV, except that J0720 shows a broad case ($\sigma \gtrsim 1$ keV). We also fit the spectrum of J0720 with the nonuniform model plus a power law emission. However, the fact that it has a high-energy tail, surprisingly close to a Wien spectrum (van Kerkwijk et al. 2007), suggests the spectrum does not have nonthermal (i.e., power law) components. Therefore, this broad line may be composed of multiple absorption lines.

A normal NS atmosphere is supposed to be on top of a condensed surface (Ho et al. 2007). However, the condensed surface is suggested to be maintained by a strong magnetic field ($\sim 10^{13}$ G, Lai 2001). In this case, some absorption features would be exhibited in the X-ray spectrum of J1856, but not detected with certainty. In addition, this condensed surface, described as an additional "modified" blackbody (Ho et al. 2007), radiates more low-energy photons so that a large value of $N_{\rm H}$ has to be introduced that would consequently present strong photoelectric absorption. The spectral deviation, which is not an observational error, is unlikely to originate from a uniform NS atmosphere. The nonuniformity of the atmosphere, which is demonstrated by the X-ray pulsation, cannot be understood in the frame of some processes created in the NS atmosphere (e.g., Chang & Bildsten 2003).

4.3 Infrared Observations of XDINS

Infrared (IR) observations are very important for understanding the surroundings of NSs (e.g., disks around isolated NSs, Wang et al. 2006, 2014). Accretion disks around magnetars are supported by X-ray spectral and timing observations, as well as radio, optical and IR observations (e.g., Trümper et al. 2013). Thus, XDINSs and magnetars which are rotating slowly as well as some highly magnetic NSs are considered the most promising places to find fallback disks. Even though the luminosities of XDINSs are less than those of magnetars, XDINSs might also have comparable near IR emission (see fig. 2 in Mignani et al. 2008).

IR observations have shown that dusty asteroid belts may surround J0806 and J2143 rather than thin dusty disks (Posselt et al. 2014). For the five other known XDINSs, there is still no significant evidence of warm or cold dust emission. A possible reason for the missing disks is that they have never had disks since they were born or only small dust grains could be close, making them appear that they lost disks (Posselt et al. 2014). Spherical Bondi accretion cannot provide a strong braking torque during stellar evolution. If XDINSs occur during a "transitional" disk, the IR radiation may be ab-

sorbed by the geometrically thick disk, which explains the evaporated thin disk. A dense ISM environment of $\sim 10^3\,\mathrm{cm}^{-3}$ is needed.

For J2143, emission from a position on the NS consists of a blend of at least one southern and one brighter northern source, as observed by the red Photodetector Array Camera and Spectrometer (PACS; Poglitsch et al. 2010) band, but it is very faint emission northwest of the NS in the blue PACS band (see fig. 5 in Posselt et al. 2014). The belt as well as these "positional disturbances" may result in the flat spectrum at optical bands. Lo Curto et al. (2007) show that the upper limits of IR flux derived by VLT observations are well above those extrapolated from the X-ray spectrum. To better constrain the optical/NIR emission properties of XDINSs, much deeper observations are still needed. After around 5 years, the IR properties of XIDNS should be able to be detected by the Large Optical Telescope (LOT).

4.4 Geometry of XDINS

A rotating NS with a nonuniform plasma atmosphere could emit pulsed emissions which would be observed. In this case, the PF depends on the inclination angle α (see fig. A.1) which tends to align in the regime of the wind braking (Tong & Kou 2017). It is assumed that the discovered Hα nebula (see van Kerkwijk & Kulkarni 2001b) is powered by magnetic dipole braking. Roughly an age for the NS of $\sim 5 \times 10^5$ years is calculated for J1856 from its proper motion. Thus, as shown in the pulsar $P - \dot{P}$ diagram, there may be some evolutionary links between XDINSs and magnetars. For instance, J1856 may be in a state of wind braking before it shows purely thermal emission (Tong & Kou 2017). This may indicate that XDINS may be the result of magnetar evolution (i.e., an anti-magnetar which is radio-silent but emitting X-rays).

To constrain the geometry of XDINS, the two angles (α and ζ) could be calculated through measured pulsations and polarizations. The results of X-ray pulsation measurement are shown in Table 1, but measurements of the polarization in soft X-rays are not feasible yet. However, X-ray polarization properties are very significant for detecting an NS's magnetic field and constraining the properties of its surface (e.g., González Caniulef et al. 2016) as well as testing the model presented in this paper. A pulse profile can also detect the particle distribution. Moreover, both optical pulsations and polarization measurements are very difficult to reach for quite faint targets, like the Seven which have optical counterparts with magnitudes $\sim 26 - 28$. Only one of the seven, J1856, has been detected with optical linear polarization (Mignani et al. 2017) which indicates a magnetic field of $B \sim 10^{13}\,\mathrm{G}$. However, the properties of X-ray polarization may be different from those of optical polarization, which results from X-ray and optical emission coming from different positions with different optical depths. The X-ray polarization properties are expected to be tested by the Lightweight Asymmetry and Magnetism Probe (LAMP), which is supposed to work in conjunction with China's space station around 2020 (She et al. 2015).

5 SUMMARY

In this paper, we presented a radiative model of a nonuniform plasma atmosphere applicable to a strangeon star's surface that has negligible emission, and proposed that the observed emission is bremsstrahlung radiation from the atmosphere. The accreted matter moves along the magnetic field lines to near the polar caps, and may diffuse to other parts, making the atmosphere nonuniform. This allows us to understand how the spectral index deviates from the expected R-J spectrum and the X-ray pulsations as well as the optical/UV excess of XDINS. The spectra of five XDINSs (J0720, J0806, J1308, J1605 and J1856) would be fitted well in the radiative model, from X-ray to optical/UV bands, exhibiting Gaussian like absorption lines. The results of data fitting show that the electron temperatures are $\sim 100 - 200\,\mathrm{eV}$ and that the radiation radii are $\sim 5 - 14\,\mathrm{km}$.

Acknowledgements We are grateful to Hao Tong at Guangzhou University for discussions. W.Y.W. and X.L.C. acknowledge the support of MoST (2016YFE0100300) and the National Natural Science Foundation of China (NSFC, Nos. 11473044, 11633004, 11653003) and CAS (QYZDJ-SSW-SLH017). Y.F. is supported by the Open Project Program of the Key Laboratory of FAST, Chinese Academy of Sciences (CAS). X.Y.L. is supported by the West Light Foundation (XBBS-2014-23) and NSFC (No. 11203018). J.G.L is supported by NSFC (No. 11225314) and the Open Project Program of the Key Laboratory of Radio Astronomy, CAS. Y.Y.L. and R.X.X. are supported by the National Key R&D Program of China (No. 2017YFA0402602), NSFC (Nos. 11673002 and U1531243) and the Strategic Priority Research

Program of CAS (No. XDB23010200). The FAST FELLOWSHIP is supported by Special Funding for Advanced Users, budgeted and administrated by the Center for Astronomical Mega-Science, Chinese Academy of Sciences (CAMS).

Appendix A: APPENDIX: FLUX OF BREMSSTRAHLUNG FROM A ROTATING NS

In the corotating coordinate frame (x, y, z), $P[P = (\theta, \phi)$, unit vector $\boldsymbol{n}]$ is the emission point on the NS's surface, and two angles ζ and α are defined: the former is the angle between the line of sight (LOS) and the spin axis $\boldsymbol{\Omega_s}$ which is in the $\hat{x}\hat{z}$-plane, where the z-axis is parallel to the magnetic (dipole) axis, while the latter is the inclination angle between the magnetic axis (a dipole magnetic field is assumed) and the spin axis. Also, a fixed coordinate system (X, Y, Z) is introduced with the Z-axis parallel to LOS and the X-axis in the LOS-spin plane. The associated polar angles are $(\Theta_{\rm S}, \Phi_{\rm S})$ in the fixed coordinate, respectively. The transformations linking the pairs of polar angles in the two systems are (see Zane & Turolla 2006)

$$\begin{cases} \cos\theta = \boldsymbol{n}\cdot\boldsymbol{b}\,, \\ \cos\phi = \boldsymbol{n}_\perp\cdot\boldsymbol{q}_\perp\,, \end{cases} \tag{A.1}$$

where $\boldsymbol{n} = (\sin\Theta_{\rm S}\cos\Phi_{\rm S}, \sin\Theta_{\rm S}\sin\Phi_{\rm S}, \cos\Phi_{\rm S})$, $\boldsymbol{b} = (\sin\zeta\cos\alpha - \cos\zeta\sin\alpha\cos\omega t, \sin\alpha\sin\omega t, \cos\zeta\sin\alpha + \sin\zeta\sin\alpha\cos\omega t)$ is the magnetic axis in the fixed frame (here $\omega = 2\pi/P$ is the angular velocity), an additional vector $\boldsymbol{q} = (-\cos\zeta\cos\omega t, \sin\omega t, \sin\zeta\cos\omega t)$, the component of $\boldsymbol{q}$ perpendicular to $\boldsymbol{b}$

$$\boldsymbol{q}_\perp = \frac{\boldsymbol{q} - (\boldsymbol{b}\cdot\boldsymbol{q})\boldsymbol{b}}{(1-\boldsymbol{b}\cdot\boldsymbol{q})^{\frac{1}{2}}}, \tag{A.2}$$

and $\boldsymbol{n}_\perp$ is defined in analogy with $\boldsymbol{q}_\perp$.

The emission from a local region on a rotating NS is illustrated in Figure A.1. Its flux, averaged over a long timescale T, could be described as

$$\bar{F}_\nu = \frac{1}{T}\int_0^T {\rm d}t \int I_\nu \cos\Theta_{\rm S}{\rm d}\Omega, \tag{A.3}$$

where I_ν is the specific intensity and ${\rm d}\Omega$ is the solid angle in the fixed coordinate. In the following calculations, it is assumed that the density of the strangeon star is $1.5\times2.8\times10^{14}\,{\rm cm}^{-3}$ and the atmosphere is mainly composed of hydrogen ($m_{\rm i}\sim1\,{\rm GeV}/c^2$). The observed time

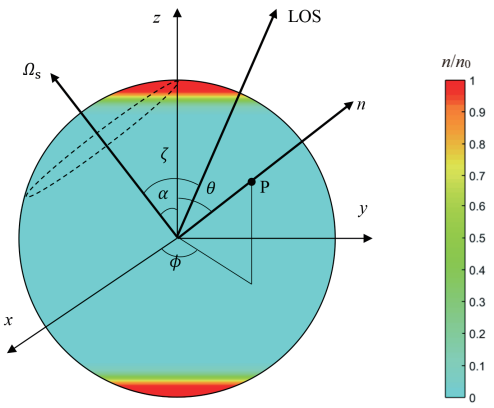

Fig. A.1 Coordinate axes and angles used to describe the geometry and pulsed emission as well as the distribution, represented by color, of the plasma atmosphere number density. The *dashed line* indicates the position of the magnetic pole $\boldsymbol{b}$ as the NS rotates about $\boldsymbol{\Omega}_{\rm S}$. The parameters describing the number density of electrons are $\xi = 150, \gamma = 3$.

averaged radiation should be gravitationally redshifted, i.e.,

$$\bar{F}_\nu^\infty \simeq F_{\nu0} + \pi\left(\frac{R_{\rm opt}^\infty}{d}\right)^2\frac{B_\nu}{T} \int_0^T {\rm d}t\int\left[1-\exp(-\tau_\nu^\infty)\right]{\rm d}\Omega, \tag{A.4}$$

where $R_{\rm opt}^\infty$ is the radiation radius, d is the distance from the source, B_ν is the Planck function, $F_{\nu0}$ is the flux from a bare strangeon star which can be calculated to be

$$\pi\left(\frac{R_{\rm opt}^\infty}{d}\right)^2\frac{B_\nu}{T}\exp\left(-\tau_\nu^\infty\right)\int_0^T {\rm d}t\int[1-\exp(-\tau_\nu^\infty)]{\rm d}\Omega, \tag{A.5}$$

and $\tau_\infty(\nu)$ is the observed optical depth at far field which can be described as

$$\tau_\infty(\nu) = \frac{8\pi\sqrt{2}h^2n_{\rm i0}^2(\theta)e^6kT_{\rm i}}{3m_{\rm e}^{1.5}(h\nu)^{3.5}m_{\rm i}gc}\left[1-\exp\left(-\frac{h\nu}{kT_{\rm e}}\right)\right]$$
$$= 3.92\times10^{-45}\frac{n_{\rm i0}^2(\theta)(kT_{\rm i})_{\rm keV}}{(h\nu)_{\rm keV}^{3.5}R_{\rm km}}\left[1-\exp\left(-\frac{h\nu}{kT_{\rm e}}\right)\right], \tag{A.6}$$

where h is the Planck constant, $m_{\rm e}$ is the mass of an electron, $T_{\rm e}$ is the temperature of electrons, e is elementary charge and c is the speed of light.

References

Abbott, B. P., Abbott, R., Abbott, T. D., et al. 2017, Physical Review Letters, 119, 161101

Alcock, C., Farhi, E., & Olinto, A. 1986, ApJ, 310, 261

Annala, E., Gorda, T., Kurkela, A., & Vuorinen, A. 2017, arXiv:1711.02644

Arnaud, K. A. 1996, in Astronomical Society of the Pacific Conference Series, 101, Astronomical Data Analysis Software and Systems V, ed. G. H. Jacoby & J. Barnes, 17
Burwitz, V., Zavlin, V. E., Neuhäuser, R., et al. 2001, A&A, 379, L35
Burwitz, V., Haberl, F., Neuhäuser, R., et al. 2003, A&A, 399, 1109
Cardelli, J. A., & Ackerman, T. P. 1983, PASP, 95, 451
Chang, P., & Bildsten, L. 2003, ApJ, 585, 464
Chatterjee, P., Hernquist, L., & Narayan, R. 2000, ApJ, 534, 373
Davidson, K., & Ostriker, J. P. 1973, ApJ, 179, 585
Geppert, U., Küker, M., & Page, D. 2006, A&A, 457, 937
Goldreich, P., & Julian, W. H. 1969, ApJ, 157, 869
González Caniulef, D., Zane, S., Taverna, R., Turolla, R., & Wu, K. 2016, MNRAS, 459, 3585
Haberl, F., Zavlin, V. E., Trümper, J., & Burwitz, V. 2004, A&A, 419, 1077
Haberl, F. 2007, Ap&SS, 308, 181
Ho, W. C. G., Kaplan, D. L., Chang, P., van Adelsberg, M., & Potekhin, A. Y. 2007, MNRAS, 375, 821
Illarionov, A. F., & Sunyaev, R. A. 1975, A&A, 39, 185
Kalberla, P. M. W., Burton, W. B., Hartmann, D., et al. 2005, A&A, 440, 775
Kaplan, D. L., Kamble, A., van Kerkwijk, M. H., & Ho, W. C. G. 2011, ApJ, 736, 117
Kaplan, D. L., & van Kerkwijk, M. H. 2005, ApJ, 635, L65
Kaplan, D. L., & van Kerkwijk, M. H. 2009, ApJ, 705, 798
Lai, D. 2001, RvMP, 73, 629 (astro-ph/0009333)
Lai, X., & Xu, R. 2017, in Journal of Physics Conference Series, 861, 012027
Liu, X.-W., Xu, R.-X., Qiao, G.-J., Han, J.-L., & Tong, H. 2014, RAA (Research in Astronomy and Astrophysics), 14, 85
Lo Curto, G., Mignani, R. P., Perna, R., & Israel, G. L. 2007, A&A, 473, 539
Long, M., Romanova, M. M., & Lovelace, R. V. E. 2007, MNRAS, 374, 436
Menou, K., Esin, A. A., Narayan, R., et al. 1999, ApJ, 520, 276
Mignani, R. P., Falomo, R., Moretti, A., et al. 2008, A&A, 488, 267
Mignani, R. P., Testa, V., González Caniulef, D., et al. 2017, MNRAS, 465, 492
Mori, K., & Ruderman, M. A. 2003, ApJ, 592, L75
Morrison, R., & McCammon, D. 1983, ApJ, 270, 119
Mueller, E. 1984, A&A, 130, 415
Poglitsch, A., Waelkens, C., Geis, N., et al. 2010, A&A, 518, L2
Pons, J. A., Miralles, J. A., & Geppert, U. 2009, A&A, 496, 207
Posselt, B., Pavlov, G. G., Popov, S., & Wachter, S. 2014, ApJS, 215, 3
Potekhin, A. Y., Ho, W. C. G., & Chabrier, G. 2016, arXiv:1605.01281
Predehl, P., & Schmitt, J. H. M. M. 1995, A&A, 293, 889
Romanova, M. M., Blinova, A. A., Ustyugova, G. V., Koldoba, A. V., & Lovelace, R. V. E. 2018, New Astron., 62, 94
She, R., Feng, H., Muleri, F., et al. 2015, in Proc. SPIE, 9601, UV, X-Ray, and Gamma-Ray Space Instrumentation for Astronomy XIX, 96010I
Tong, H. 2016, Science China Physics, Mechanics, and Astronomy, 59, 5752
Tong, H., & Kou, F. F. 2017, ApJ, 837, 117
Toropina, O. D., Romanova, M. M., Toropin, Y. M., & Lovelace, R. V. E. 2001, ApJ, 561, 964
Trümper, J. E., Burwitz, V., Haberl, F., & Zavlin, V. E. 2004, Nuclear Physics B Proceedings Supplements, 132, 560
Trümper, J. E., Dennerl, K., Kylafis, N. D., Ertan, Ü., & Zezas, A. 2013, ApJ, 764, 49
Turolla, R. 2009, in Astrophysics and Space Science Library, 357, ed. W. Becker, 141
Turolla, R., Zane, S., & Drake, J. J. 2004, ApJ, 603, 265
Usov, V. V. 2001, ApJ, 550, L179
van Kerkwijk, M. H., & Kaplan, D. L. 2007, Ap&SS, 308, 191
van Kerkwijk, M. H., Kaplan, D. L., Pavlov, G. G., & Mori, K. 2007, ApJ, 659, L149
van Kerkwijk, M. H., & Kulkarni, S. R. 2001a, A&A, 378, 986
van Kerkwijk, M. H., & Kulkarni, S. R. 2001b, A&A, 380, 221
Wang, Z., Chakrabarty, D., & Kaplan, D. L. 2006, Nature, 440, 772
Wang, Z., Ng, C.-Y., Wang, X., Li, A., & Kaplan, D. L. 2014, ApJ, 793, 89
Wang, W., Lu, J., Tong, H., et al. 2017, ApJ, 837, 81
Xu, R.-X. 2014, RAA (Research in Astronomy and Astrophysics), 14, 617
Xu, R. X., Bastrukov, S. I., Weber, F., Yu, J. W., & Molodtsova, I. V. 2012, Phys. Rev. D, 85, 023008
Zane, S., & Turolla, R. 2006, MNRAS, 366, 727